Return to C Dixon
At [illegible] back to
photo

CANADA

DEPARTMENT OF ENERGY, MINES AND RESOURCES

MINES BRANCH

OTTAWA

PHYSICAL METALLURGY DIVISION

INTERNAL REPORT PM-R-68-9

A STUDY OF THE PROPERTIES AND SINTERING BEHAVIOUR OF CERTAIN NICKEL POWDERS

PROGRESS REPORT NO. 1

by

H. M. Skelly and C. F. Dixon

Nuclear and Powder Metallurgy Section

23 April 1968

Internal Report PM-R-68-9

A STUDY OF THE PROPERTIES AND SINTERING BEHAVIOUR OF CERTAIN NICKEL POWDERS
- PROGRESS REPORT NO. 1 -

by

H. M. Skelly* and C. F. Dixon**

- - - - - - -

ABSTRACT

The physical properties and sintering behaviour of eight samples of nickel powder having widely differing particle characteristics were studied.

The apparent density, flow rate, particle size and shape, and microstructure of the powders were investigated.

Sintering behaviour was studied by heating uncompacted and compacted samples at 1105°C (2025°F) for periods of 2 and 4 hours.

The density and porosity of the sintered powders were measured and their microstructures examined.

---

* Research Scientist and ** Scientific Officer, Nuclear and Powder Metallurgy Section, Physical Metallurgy Division, Mines Branch, Department of Energy, Mines and Resources, Ottawa, Canada.

CONTENTS

		Page
i	Abstract	i
1.	Introduction	1
2.	Test Material	1
3.	Experimental Procedure	2
4.	Experimental Results	3
	4.1 Properties of Powders	3
	4.2 Sintering of Uncompacted Powders	4
	4.3 Sintering of Compacted Powders	4
5.	Discussion of Results	5
	5.1 Properties of Powders	5
	5.2 Sintering of Uncompacted Powders	5
	5.3 Sintering of Compacted Powders	7
6.	Conclusions	9
7.	Acknowledgements	9
8.	References	9
Tables 1 - 6		10 to 12
Figures 1 - 26		13 to 27

1. INTRODUCTION

The work reported here deals with some aspects of the influence of particle morphology on the sintering behaviour of nickel powders and is part of a larger research project encompassing the fundamentals of powder metallurgy.

The size and shape of individual metal powder particles influence the apparent density and flow rate of the bulk powder. These properties in turn control the powder's die-filling and compacting characteristics, both of which are important in production operations.

Sintering transforms the fragile green compact into a coherent mass possessing useful mechanical strength. Numerous theories of sintering have been proposed and although there has been no general acceptance of any one theory, it is acknowledged that several processes (i.e., viscous flow, plastic flow, volume diffusion, surface diffusion and evaporation-condensation) are probably involved. Important practical factors in the sintering process are time and temperature, but sintering is also influenced by the form, size, condition, and degree of contact of the powder particles.

Nickel powders were chosen for this initial work because of their ready availability in a variety of forms from a Canadian source which produces nickel by precipitation from solution as pure powder.

Future work will include a study of nickel powder produced by other methods such as the carbonyl process.

2. TEST MATERIAL

The manufacturer's * designation and published characteristics of the nickel powders were as follows:

---

* Sherritt Gordon Mines Limited.

Grade	Particle Features	Particle Size U.S. Sieve No.	Fisher No.
S	Spheroidal. Pebbly	(See below)	-
SF300	Spheroidal. Irregular	-325:99%	19.2
OSF100x150	Spherical. Smooth	+100:7%	-
		-100+150:91.5%	
		-150:1.5%	
OSF 20x35	Spherical. Smooth	- 20+ 35:93.5%	-
		- 35:6.5%	
G-08	Dendritic. Agglomerate	-325:97%	2.8
G-29	Dendritic. Agglomerate	-325:98%	6.4

The S grade powder gave the following sieve analysis:

U.S. Sieve Nos.	+80	-80 +100	-100 +140	-140 +200	-200 +230	-230 +325	-325
Wt.% retained.	0.3	0.9	18.6	28.4	16.4	20.6	14.8

In addition to the above powders, the -100+140 mesh and -325 mesh fractions of the S grade powder were investigated, the fractions being obtained by screening them from the S powder.

The chemical analyses of the powders are listed in Table 1. The comparatively high hydrogen loss values for G-08 and G-29 are probably a consequence of the large surface area of the powders, resulting in greater than average superficial oxidation.

3. EXPERIMENTAL PROCEDURE

Flow rate of the powders was determined in accordance with Metal Powder Industries Federation (MPIF) Standard No. 3-45 in which the time taken for 50g of powder to flow through a Hall Flowmeter funnel is measured. The apparent density was determined by MPIF Standard No. 4-45 for free-flowing powders, using a Hall Flowmeter funnel, and by MPIF Standard No. 28-59 for non-free-flowing powders, using a Carney funnel.

Green density was determined by calculation from the dimensions and weight of the compact (MPIF Standard No. 13-62).

Sintered density was determined by two methods: (a) impregnating the compact with oil and weighing in air and water, and (b) coating the compact with lacquer and weighing in air and water (MPIF Standard No. 8-50). Good agreement was obtained between the two methods.

Interconnected porosity in sintered compacts was measured from the volume of oil absorbed by the compact (MPIF Standard No. 8-50). The total porosity was calculated from the "true" density of nickel (8.90 g/cc) and the actual density of the compact, making the assumption that the difference in the two densities was due solely to porosity.

Compaction of the powders prior to sintering was carried out in a 100-ton hydraulic press. The powders were compressed in a double-acting die designed to prepare tensile test specimens to the dimensions specified in MPIF Standard No. 10-50. No lubricant was added to the powders, but the die walls were lubricated with stearic acid.

Sintering tests were also made on non-compacted powders poured into graphite moulds containing a cavity with the same dimensions as those of the tensile test die.

Sintering was carried out at 1105°C (2025°F) for times of 2 and 4 hours in a molybdenum-wound resistance furnace using an atmosphere of bottled hydrogen.

Two methods were used to mount the loose powders for polishing prior to metallographic examination. In one, used for the extra-fine powders G-08 and G-29, the samples were mixed with Eastman 910 adhesive and the resulting paste was poured over the grooved face of a bakelite mount; the adhesive was then allowed to set at room temperature. In the other method, the powder was mixed with Buehler AB plastic epoxide to give a slurry which was then poured into a steel retaining ring and allowed to set at room temperature.

For metallographic examination of the sintered powders, the specimens were impregnated with the plastic epoxide under vacuum and then mounted in the epoxide.

The surface preparation procedure for microexamination was first to grind on emery paper to 4/0 grit and then to polish with Linde A and Linde B compounds on silk cloth, finishing with magnesium oxide on gamal cloth.

Etching was carried out with a solution of 5 to 10 ml nitric acid in 10 ml water, the strength depending on the nature of the specimen.

4. EXPERIMENTAL RESULTS

4.1 Properties of Powders

The appearance of the powder particles is illustrated in Figures 1 to 8.

The S grade powder (Figure 1) consists of particles with a pebbly surface and a wide range in size. The -100+140 and -325 fractions of the S grade powder are illustrated in Figures 2 and 3, respectively. The SF300 grade powder (see Figure 4) exhibits a pebbly surface similar to that of the S grade, and is probably equivalent to the -325 fraction of S. The two OSF grades of powder (see Figures 5 and 6) consist of spherical particles with smooth surfaces. The G-08 and G-29 powders consist of irregular-shaped dendritic particles; they are shown at two magnifications in Figures 7 and 8.

Samples of the powders were mounted, polished and etched to reveal their microstructures, which are illustrated in Figures 9 to 16. The similarity between the three S powders (Figures 9, 10 and 11) and the SF300 powder (Figure 12) can be seen - the irregular outer surface and the cored interior. The smooth, rounded surface of the OSF powders is evident in Figures 13 and 14; the cored structure, which is very clear in these illustrations, is more regular in OSF 20 x 35 (Figure 14) than in OSF 100x150 (Figure 13). The small particle size of the G powders and a tendency to agglomerate made them difficult to photograph, but Figures 15 and 16 give some indication of the size and structure of the particles.

The flow rate and apparent density of the powders are listed in Table 2. The G-08 and G-29 powders exhibited nil flow rate.

4.2 Sintering of Uncompacted Powders

Samples from each of the eight lots of powder were sintered uncompacted for 2 and 4 hours at 1105°C (2025°F). The densities of the sintered specimens are listed in Table 3 and the total and interconnected porosities in Table 4. The variation of density with sintering time is plotted in Figure 17, using the apparent density of the unsintered powders as the first point on the plots. Representative microstructures of the sintered specimens are shown in Figures 18 to 22.

4.3 Sintering of Compacted Powders

The number of powders was reduced for the compaction experiments. The two OSF powders could not be compacted in the usual manner and had to be omitted. G-29 was chosen as an example of a fine powder, and the other fine powders (G-08, SF300 and -325 mesh fraction of S) were excluded. This left three powders, S, -100+140 mesh fraction of S, and G-29, samples of which were compacted at 60,000 psi and sintered for 2 and 4 hours at 1105°C (2025°F).

The compression ratios of the powders at 60,000 psi were as follows:

S: 1.47 to 1
-100 + 140 mesh fraction of S: 1.46 to 1
G-29: 2.08 to 1

The densities of the compacts before and after sintering are given in Table 5. The total and interconnected porosities of the sintered compacts are listed in Table 6. The green and sintered densities are plotted against sintering time in Figure 23.

Typical microstructures of the sintered compacts are illustrated in Figures 24, 25 and 26.

5. DISCUSSION OF RESULTS

5.1 Properties of Powders

The results listed in Table 2 show that the flow rate of OSF 100 x 150 is substantially faster than that of the other powders; this can be attributed to the smooth rounded surface of the powder. Surprisingly perhaps, the other OSF powder (OSF 20 x 35) has the slowest flow rate, except of course for the two G powders, which would not flow through the orifice of the flowmeter funnel. The low rate of OSF 20 x 35 is probably a result of the comparatively large size of the particles in relation to the orifice diameter (> 0.016 in. vs 0.1 in.). Although the method used to measure flow rate is a recognized standard and has practical advantages, it does have limitations as a scientific tool.

Highest apparent density is shown by the two OSF powders (see Table 2). The two G powders have the lowest apparent densities, with that of the G-08 powder being substantially below all the others. The S and -100 + 140 fraction of S have about the same apparent density, as do the -325 fraction of S and SF300; this is not unexpected in view of the similarity between these powders.

5.2 Sintering of Uncompacted Powders

The plot of density versus sintering time for the uncompacted powders (see Figure 17) shows that after the 4 hour sinter there is only a slight increase in the density of the S powder, the -100 + 140 fraction of S and the two OSF powders. The -325 fraction of S and SF300 show an appreciable increase in density after sintering for 2 hours, and a small increase between 2 and 4 hours. The two G powders exhibit a large increase in density after the 2 hour sinter. Between 2 and 4 hours the density of the G-29 powder increases only slightly, whereas the G-08 powder shows

a significant increase in density, although at a reduced rate compared with the first 2 hours of sintering.

It is significant that the finer the particle size of the powder the greater the increase in density - the large surface area of the fine powders renders them more sinterable. The fine powders also have low apparent densities (see Table 2) and this provides more scope for an increase in density during sintering.

The porosity values listed in Table 4 are generally consistent among themselves and with the densities given in Table 3; comparing the results in Table 3 with those in Table 4, it can be seen that porosity is inversely proportional to density. The porosity results show that even after sintering for 4 hours most of the porosity is interconnected. There are one or two anomalies in the porosity results which can be attributed to experimental error, but there is one serious discrepancy in the results for G-08, which has a total porosity of 59.4% and an interconnected porosity of 66.1% after the 4 hour sinter. The reason for this discrepancy is not known, but it could be due to experimental error arising from the large amount of porosity present in the specimen.

The photomicrographs in Figures 18, 19 and 20 illustrate the microstructures of the samples whose density did not increase greatly on sintering (OSF 20 x 35 is not included as it was similar to OSF 100 x 150). The voids between the particles are considerable, but there are instances of particles coalescing. The OSF powder in Figure 20 clearly shows the formation of "necks" between particles.

Figure 21 illustrates the microstructure of the -325 fraction of the S grade nickel powder, which showed an appreciable increase in density after 4 hours of sintering (most of which occurred during the first 2 hours). This photograph shows that although some particles have coalesced there are considerable voids between the particles. (A photomicrograph of SF300 is not included as it was similar to the -325 fraction of S grade).

As shown above, the largest increase in density was exhibited by the two G powders. Their uncompacted sintered microstructure is typified by Figure 22 (G-29 powder). It can be seen that considerable coalescence of the particles has occurred.

Comparison of Figures 18 to 22 with the appearance of the corresponding powders prior to sintering (see Figures 9, 10, 11, 13 and 15) shows that during sintering grain growth occurs and internal voids open up inside the powder particles. In fact, none of the microstructures of the as-received powders (Figures 9 to 16) exhibit a crystalline structure, and it would probably be more accurate to describe the formation of a grain structure in Figures 18 to 22 as one of "crystallization" rather than "recrystallization".

The voids that open up inside the powder particles during sintering appear to be associated with inclusions or irregularities within the particles. Thus, in many cases a large void has opened up at a particle centre where most of the pre-sintered particles exhibit a distinct "nucleus" on which, presumably, the nickel was originally deposited during precipitation from solution; this relationship can be clearly seen by comparing Figures 9 and 13 with 18 and 20, respectively. Figures 18 and 20 also clearly illustrate the presence of voids at the coring striations seen in Figures 9 and 13. The voids generally tend to be of irregular contour, but there are examples of definite geometric shapes; thus, some of the particles in Figure 21 contain square voids. The latter resemble etch figures, and may be related to the crystal structure of nickel, which is face-centred cubic.

Rhines et al [1] in a study of the behaviour of porosity during sintering of copper powder observed that, although the number of pores decreased during sintering, the average pore size increased and late in the sintering process there existed pores that were larger than any present at the start of sintering. This phenomenon was explained as a vacancy diffusion mechanism - the concentration of vacancies being greater at the small pores than at the large pores, thus resulting in a flow of vacancies to the latter, where they condensed. The pores referred to by Rhines and his co-workers were inter-particle porosity rather than porosity within the particles themselves, but it is not unreasonable to expect that a similar diffusion mechanism might operate in the latter case. Another possible explanation of the voids within the particles is that, during sintering, gas dissolved in the nickel diffuses to the inclusions and irregularities, where there are free surfaces, and precipitates out of solution. It is also possible that gas might be formed during sintering by decomposition of the inclusions present within the powder particles.

5.3 Sintering of Compacted Powders

The results listed in Table 5 and plotted in Figure 23, giving the density for different sintering times, show that there is little change in the density of the two S powders even after 4 hours of sintering, but the density of the G-29 powder shows a substantial increase after 2 hours of sintering and a smaller,but still significant, increase between 2 and 4 hours.

The porosity results (see Table 6) are consistent with the density values. The two S powders contain substantial porosity, mainly inter-connected, whereas the G-29 powder contains considerably less porosity, most of which is of the closed or isolated type. (The difference between total porosity and interconnected porosity is assumed to be accounted for by closed porosity). The G-29 compacts (sintered for 2 hours and 4 hours) are the only instances where the porosity is preponderantly isolated, and are also the only examples where density approaches theoretical - being 90%

after 2 hours and 93% after 4 hours. In an investigation of permeability changes occurring on sintering copper powder, Arthur [2] found a measurable permeability at densities equal to 90% of theoretical. Permeability is proportional to interconnected porosity. The results for G-29 (compacted) show that after 4 hours of sintering, when the density is 93% of theoretical, there is 0.5% interconnected porosity, representing 7% of the total porosity (see Tables 5 and 6). However, in view of the limitations of the method used to determine porosity in this work, it is not possible to draw any firm conclusions based on the small amount of interconnected porosity measured in G-29, compacted and sintered.

The above observations are illustrated in Figures 24, 25 and 26, which are photomicrographs of the S powders after the 2 hour sinter and of the G-29 powder after the 2 and 4 hour sinters. Figures 24 and 25 illustrate that there is considerable porosity, mostly interconnected, in the S powders after sintering for 2 hours. Comparison of the microstructure of the uncompacted, sintered powders (Figures 18 and 19) with Figures 24(a) and 25(a) show that considerably more coalescence of the powder particles has occurred in the compacted specimens. It can also be seen that there are less voids between the particles of the compacted powders - this is particularly evident in the S powder (compare Figure 18 with Figure 24(a)). Comparison of Figure 24(a) with Figure 18 also shows that there is much less porosity inside the individual powder particles of the compacted sample (i.e., Figure 24(a)); this difference in internal particle porosity is not as evident in Figures 25(a) and 19. It would appear that the pressure of compaction reduces the possibility of internal voids forming in the particles during sintering. Figure 26 illustrates that most, if not all, of the porosity in the compacted and sintered G-29 is isolated and there is a significant reduction in the amount of porosity when the sintering time is increased from 2 to 4 hours.

Increased density on sintering must result from a general decrease in total porosity in both uncompacted and compacted powders. Early in the sintering process, the porosity is mainly interconnected but, as sintering proceeds, the amount of interconnected porosity decreases, resulting in an increase in closed porosity. Later in the sintering process, when the interconnected porosity has all but gone, the closed porosity tends to decrease These points are supported by the data in Tables 4 and 6. In every powder but two (S in Table 4 and G-29 in Table 6) there is a decrease in interconnected porosity between 2 and 4 hours. The result for S (Table 4) is anomalous and may be due to experimental error. G-29 (Table 6) shows no change in interconnected porosity, between 2 and 4 hours, the reason being that after two hours practically all of the porosity is of the closed type. Four powders show an increase in closed porosity between 2 and 4 hours (-100 + 140 fraction of S, OSF 100 x 150, OSF 20 x 35 in Table 4 and S in Table 6). Apart from S in Table 4, the largest decrease in closed porosity is shown by G-29 in Table 6; the latter result is illustrated by Figure 26 which shows a marked decrease in porosity, practically all closed, between 2 and 4 hours.

It is interesting to note that the increase in closed porosity between 2 and 4 hours of sintering occurs in powders with comparatively large particle size. Also, the largest increase in closed porosity occurs in the two OSF powders (see Table 4). Presumably the smooth, rounded shape of the OSF powders encourages a regular, optimum packing arrangement which favours the formation of closed porosity during sintering.

6. CONCLUSIONS

1. The increase in density of the uncompacted powders during sintering varies inversely with the particle size of the powder.

2. After sintering the uncompacted powders for 4 hours, nearly all the porosity present is interconnected.

3. Sintering of the compacted powders produces little change in density except when the particle size of the powder is fine (-325 mesh), in which case there is a substantial increase in density.

4. Most of the increase in density when the uncompacted and compacted powders are sintered occurs during the first two hours.

5. The increase in density during sintering results from a decrease in interconnected porosity with a consequent increase in closed porosity. This process continues until most of the porosity is closed and then further densification takes place by a diminution of closed porosity.

7. ACKNOWLEDGEMENTS

Mr. J. McGoey, Technical Assistant in this Section, helped with the laboratory work.

8. REFERENCES

1. F. N. Rhines, C. E. Birchenall and L. A. Hughes - "Behaviour of Pores During the Sintering of Copper Compacts", Trans. AIME 188, 378-388 (February 1950).

2. G. Arthur - "Porosity and Permeability Changes During the Sintering of Copper Powder", J. Inst. Metals 83, 329-336 (March 1954-55).

HMS/CFD/gm

TABLE 1

Chemical Analyses of Nickel Powders*

Powder	%Co	% Cu	% Fe	% S	%C	%H_2 Loss**	% Ni
S	0.050	0.003	0.019	0.017	0.005	-	Balance
SF 300	0.078	0.0065	0.16	0.013	0.007	0.19	"
OSF 100x150	0.29	0.008	0.004	0.013	0.44	-	"
OSF 20x35	0.25	0.004	0.004	0.006	0.011	-	"
G-08	0.055	0.004	0.013	0.006	0.026	0.66	"
G-29	0.047	0.006	0.012	0.004	0.033	0.53	"

* From Sherritt Gordon Mines Limited data sheets

** Weight loss after heating in hydrogen.

TABLE 2

Flow Rate and Apparent Density of Powders

Powder Samples	Flow Rate sec./50 g	Apparent Density (g/cc)
S	17.9	4.36
S, -100 + 140 fraction	18.7	4.38
S, -325 fraction	19.0	3.88
SF 300	20.6	3.48
OSF 100x150	12.2	5.20
OSF 20x35	23.0	5.41
G-08	None	0.84
G-29	None	3.06

TABLE 3

Density of Uncompacted Samples Sintered at 1105°C (2025°F)

Powder Sample	Density (g/cc)*	
	2 hr sinter	4 hr sinter
S	4.73	4.94
S, -100 + 140 fraction	4.67	4.96
S, -325 fraction	4.78	4.87
SF 300	4.43	4.83
OSF 100 x 150	5.25	5.47
OSF 20 x 35	5.50	5.50
G-08	2.88	3.61
G-29	5.56	5.70

* Determined by oil impregnation method.

TABLE 4

Porosity of Uncompacted Samples Sintered at 1105°C (2025°F)

Powder Sample	% Total Porosity		% Interconnected Porosity	
	2 hr sinter	4 hr sinter	2 hr sinter	4 hr sinter
S	46.9	44.5	43.4	44.9
S, -100 + 140 fraction	47.5	44.3	46.2	42.4
S, -325 fraction	46.3	45.3	43.4	42.9
SF 300	50.2	45.7	48.5	43.5
OSF 100 x 150	41.0	38.5	36.4	32.9
OSF 20 x 35	38.2	38.2	35.6	33.0
G-08	67.6	59.4	68.0	66.1
G-29	37.5	36.0	37.9	36.7

TABLE 5

Density of Compacts - Green and Sintered
at 1105°C (2025°F)

Powder Sample	Density (g/cc)		
	Green	2 hr sinter*	4 hr sinter*
S	6.31	6.28	6.32
S, -100 + 140 fraction	6.27	6.12	6.24
G-29	6.10	7.99	8.24

* Average of oil impregnation and lacquer coating methods.

TABLE 6

Porosity of Compacted Samples Sintered
at 1105°C (2025°F)

Powder Sample	% Total Porosity		% Interconnected Porosity	
	2 hr sinter	4 hr sinter	2 hr sinter	4 hr sinter
S	29.4	29.0	27.8	26.7
S, -100 + 140 fraction	31.2	29.9	28.3	27.8
G-29	10.2	7.4	0.4	0.5

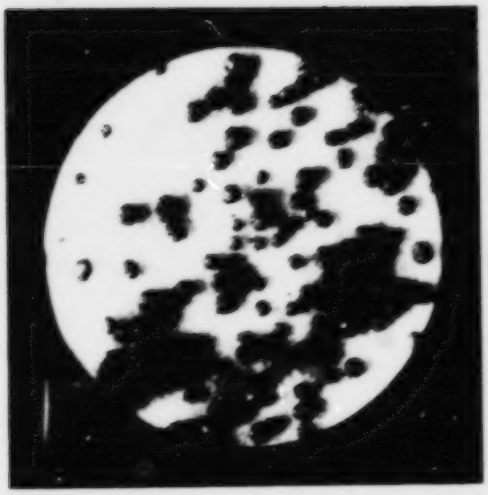

X20

Figure 1. S grade nickel powder.

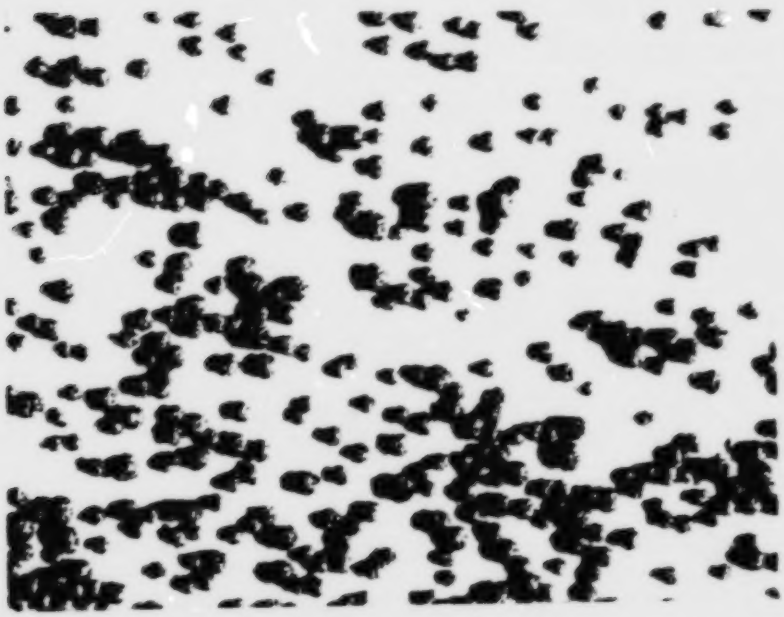

X27

Figure 2. -100 + 140 fraction of S grade nickel powder.

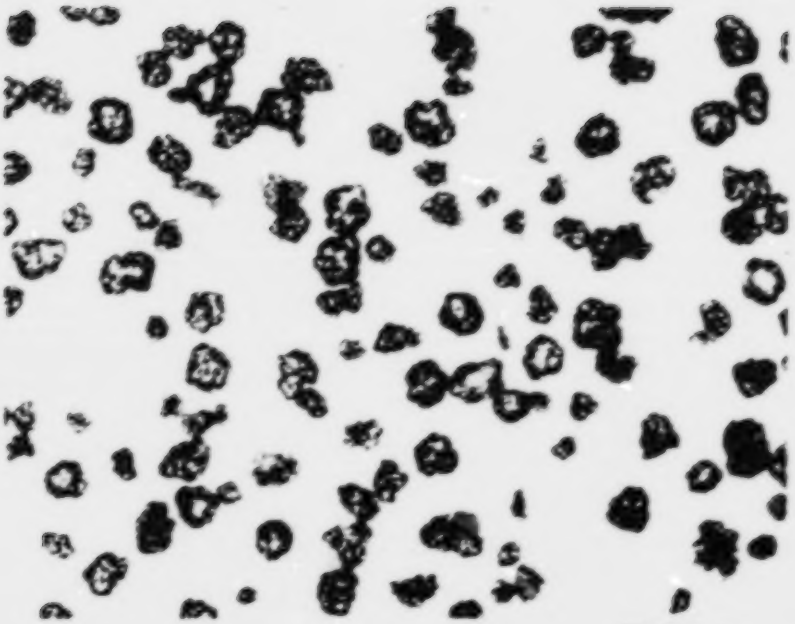

Figure 3. -325 fraction of S grade nickel powder.

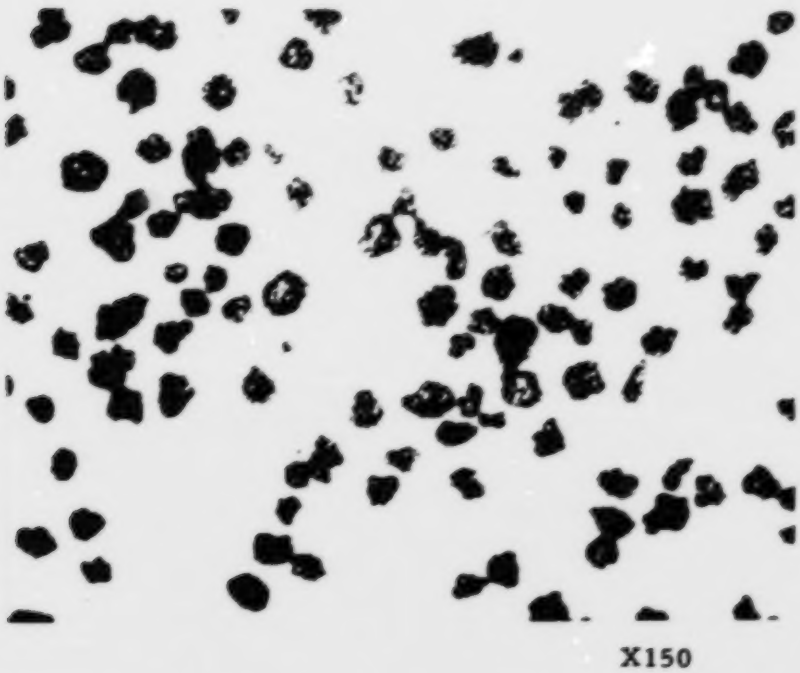

Figure 4. SF300 grade nickel powder.

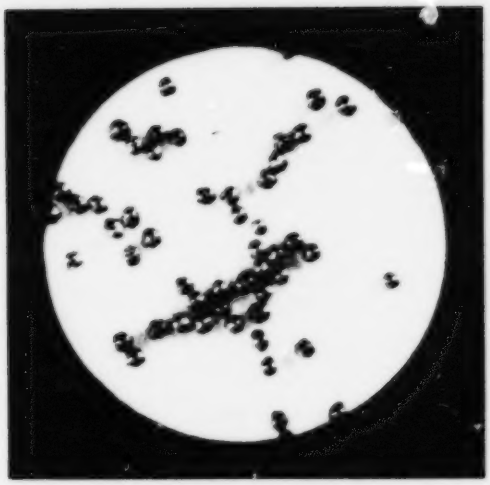

X20

Figure 5. OSF 100 x 150 grade nickel powder.

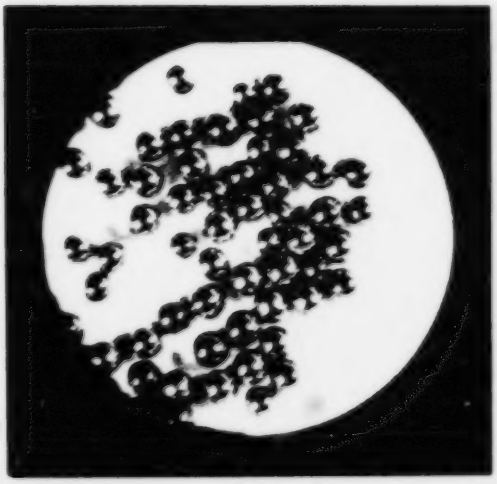

X8

Figure 6. OSF 20 x 35 grade nickel powder.

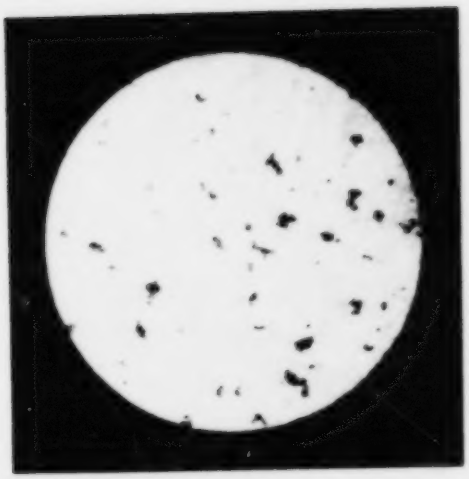

X40

(a)

X1000

(b)

Figure 7. G-08 grade nickel powder.

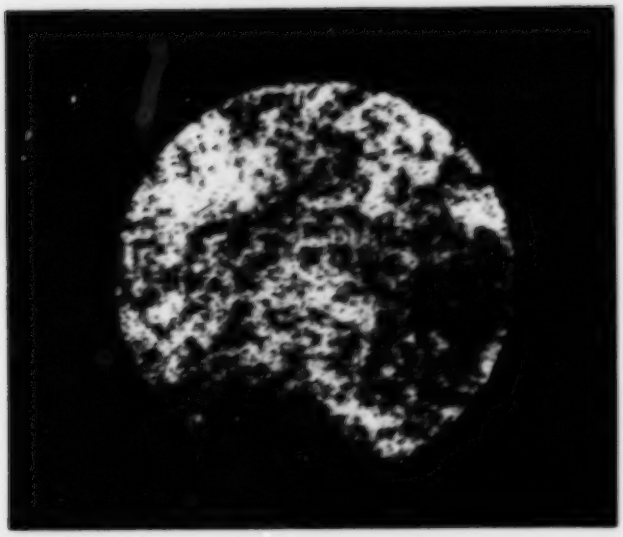

X40

(a)

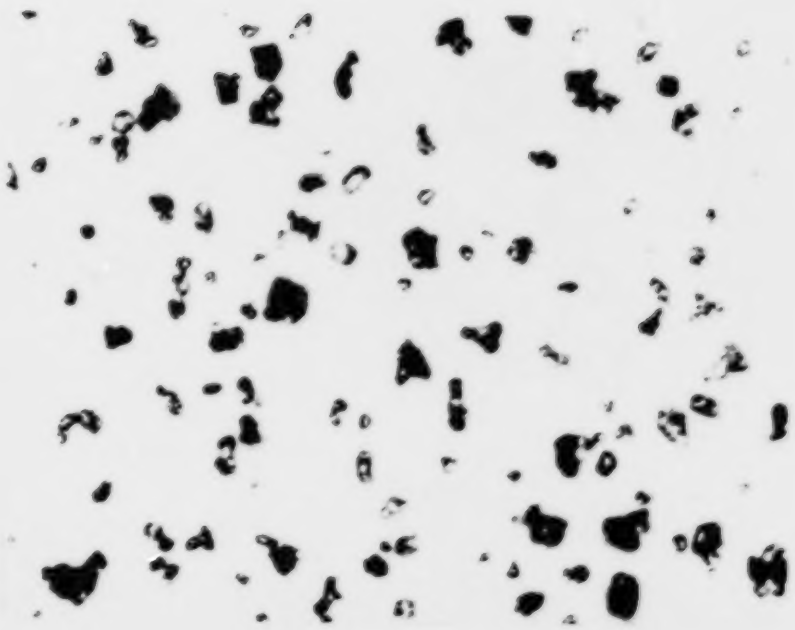

X300

(b)

Figure 8. G-29 grade nickel powder.

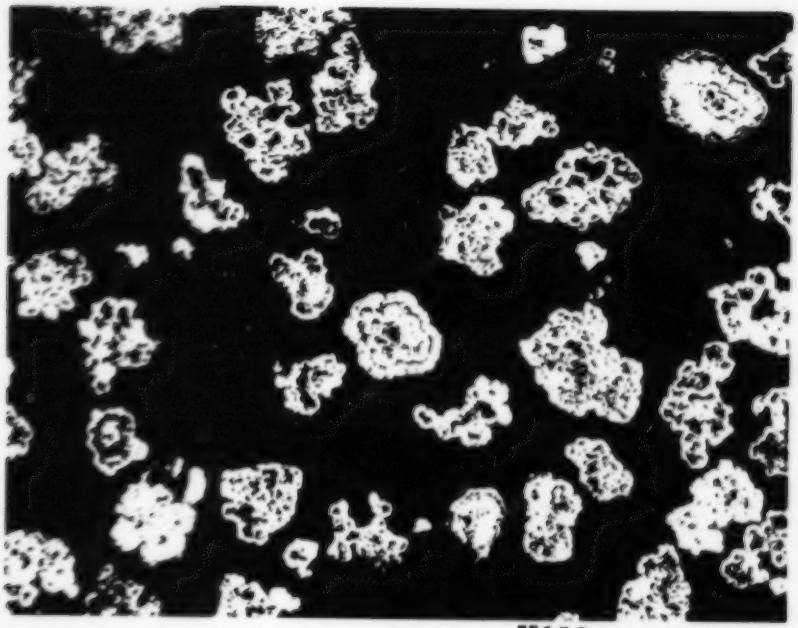

X150

Figure 9. Microstructure of S grade nickel powder. Etched.

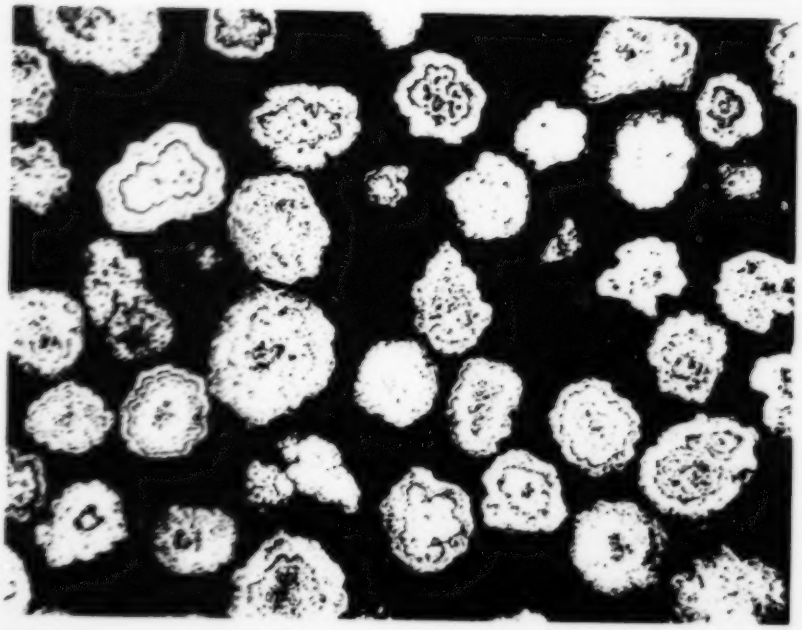

X150

Figure 10. Microstructure of -100 + 140 fraction of S grade nickel powder. Etched.

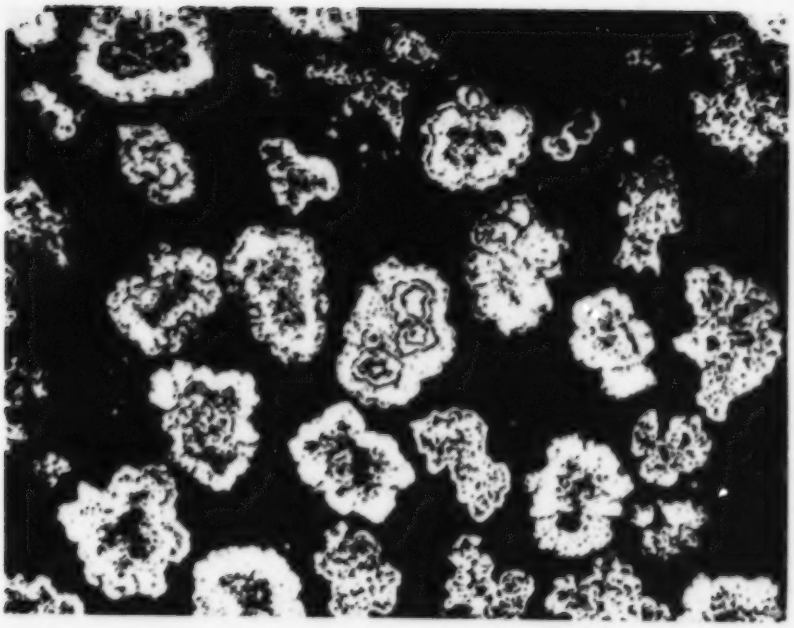

X400

Figure 11. Microstructure of -325 fraction of S grade nickel powder. Etched.

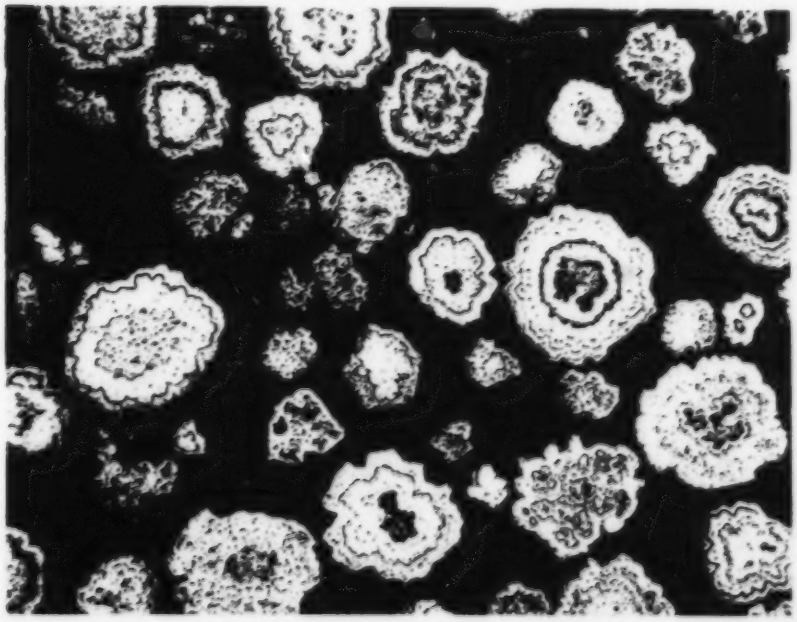

X400

Figure 12. Microstructure of SF 300 grade nickel powder. Etched.

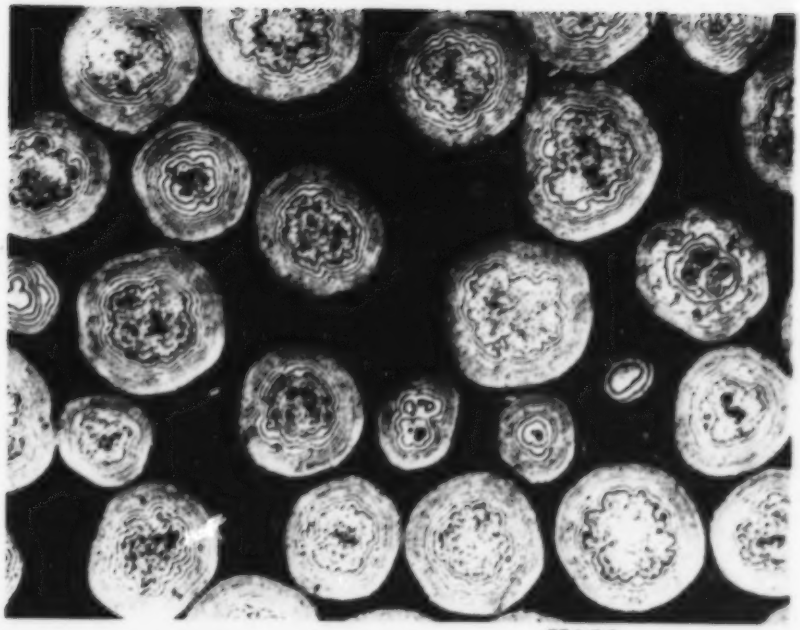

X150

Figure 13. Microstructure of OSF 100 x 150 grade nickel powder. Etched.

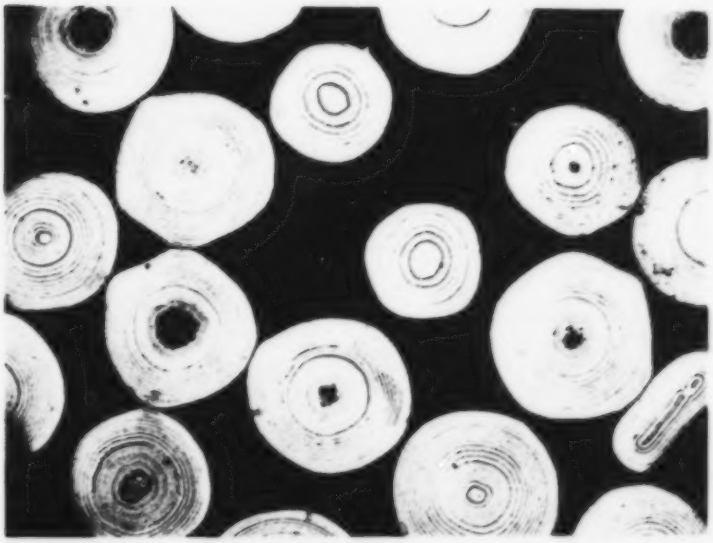

X40

Figure 14. Microstructure of OSF 20 x 35 grade nickel powder. Etched.

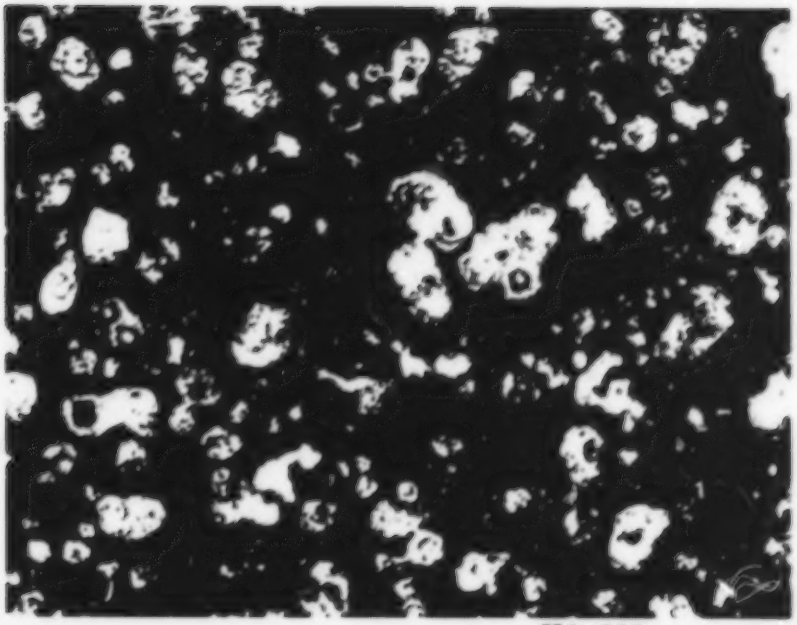

X1,000

Figure 15. Microstructure of G-29 grade nickel powder. Etched.

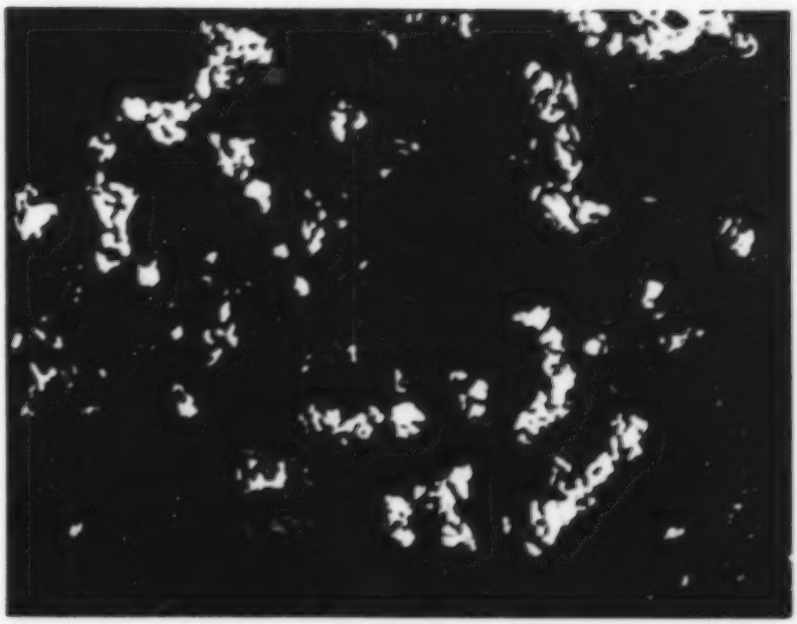

X2,000

Figure 16. Microstructure of G-08 grade nickel powder. Etched.

FIGURE 17. Density vs Sintering Time for Uncompacted Nickel Powders

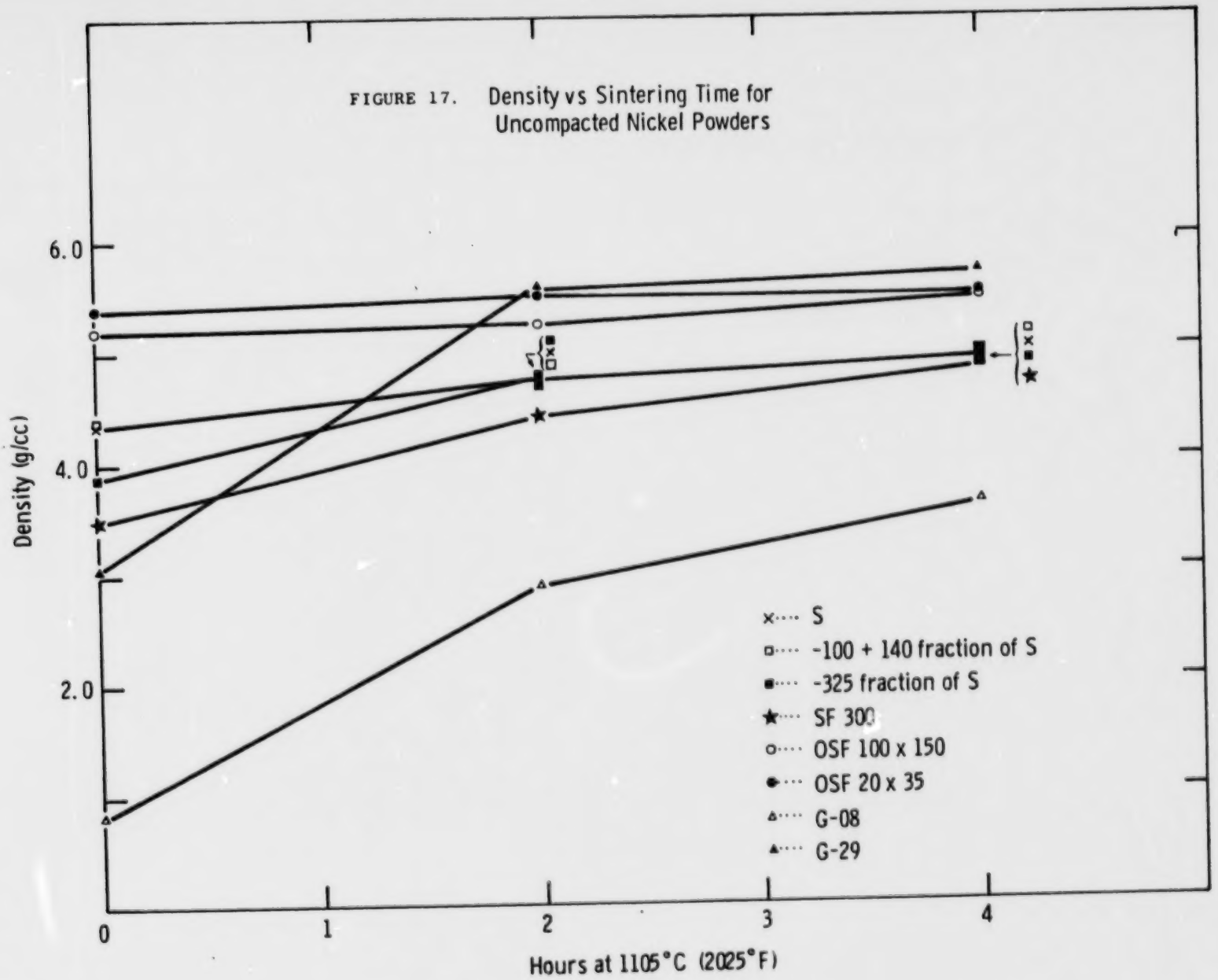

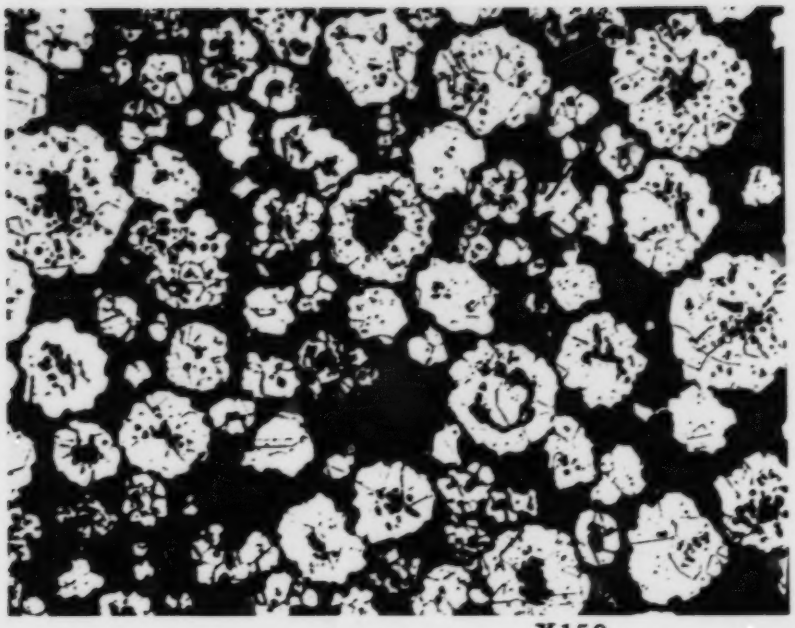

X150

Figure 18. Microstructure of S grade nickel powder. Uncompacted. Sintered at 1105°C (2025°F) for 4 hours.

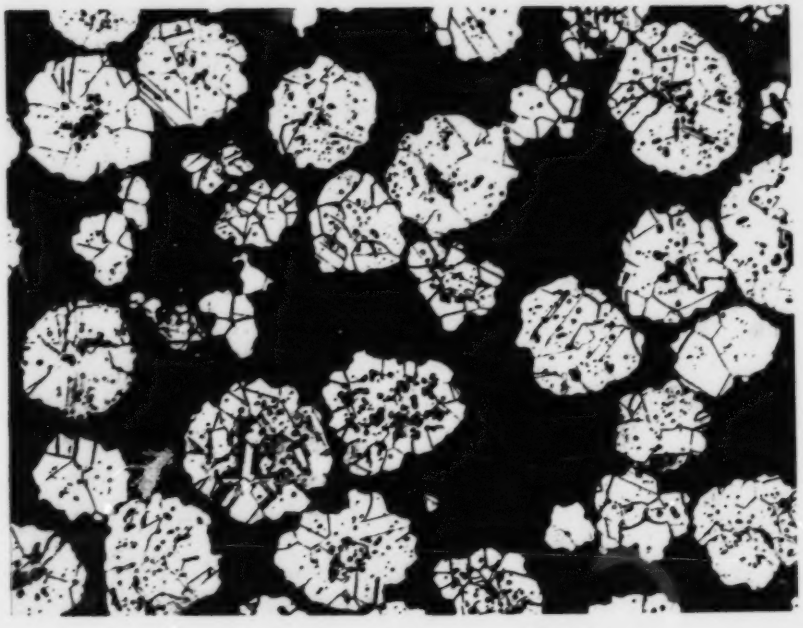

X150

Figure 19. Microstructure of -100 + 140 fraction of S grade nickel powder. Uncompacted. Sintered at 1105°C (2025°F) for 4 hours. Etched.

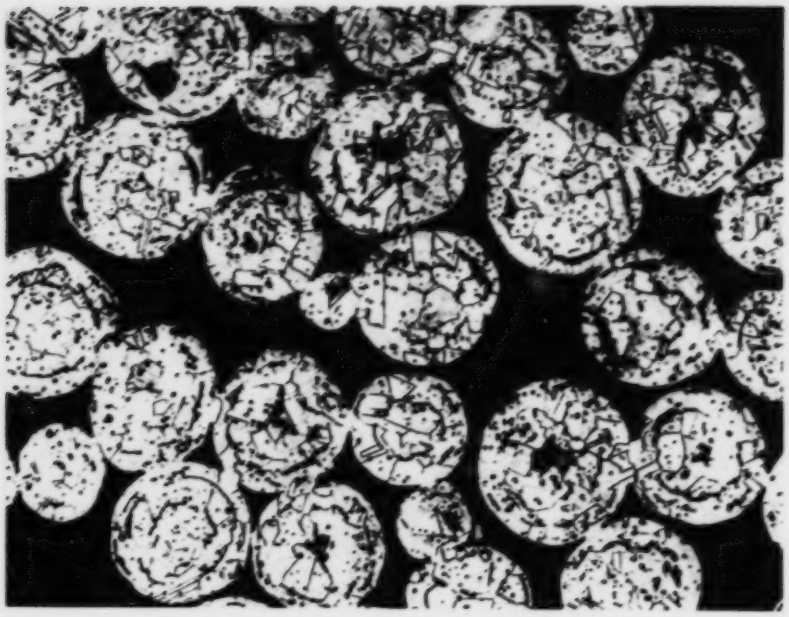

X150

Figure 20. Microstructure of OSF 100 x 150 grade nickel powder. Uncompacted. Sintered at 1105°C (2025°F) for 4 hours. Etched.

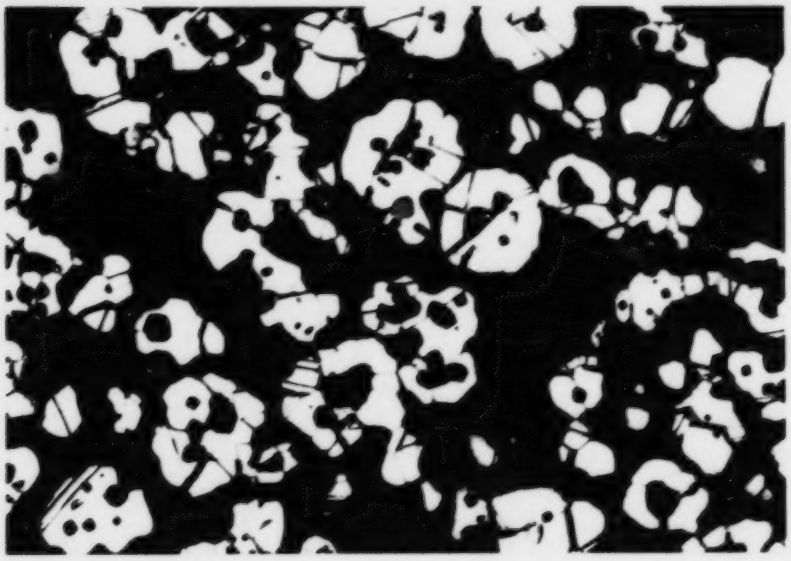

X400

Figure 21. Microstructure of -325 fraction of S grade nickel powder. Uncompacted. Sintered at 1105°C (2025°F) for 4 hours. Etched.

X500

Figure 22. Microstructure of G-29 grade nickel powder. Uncompacted. Sintered at 1105°C (2025°F) for 2 hours. Etched.

FIGURE 23. Density vs Sintering Time for Nickel Powders Compacted at 60, 000 psi

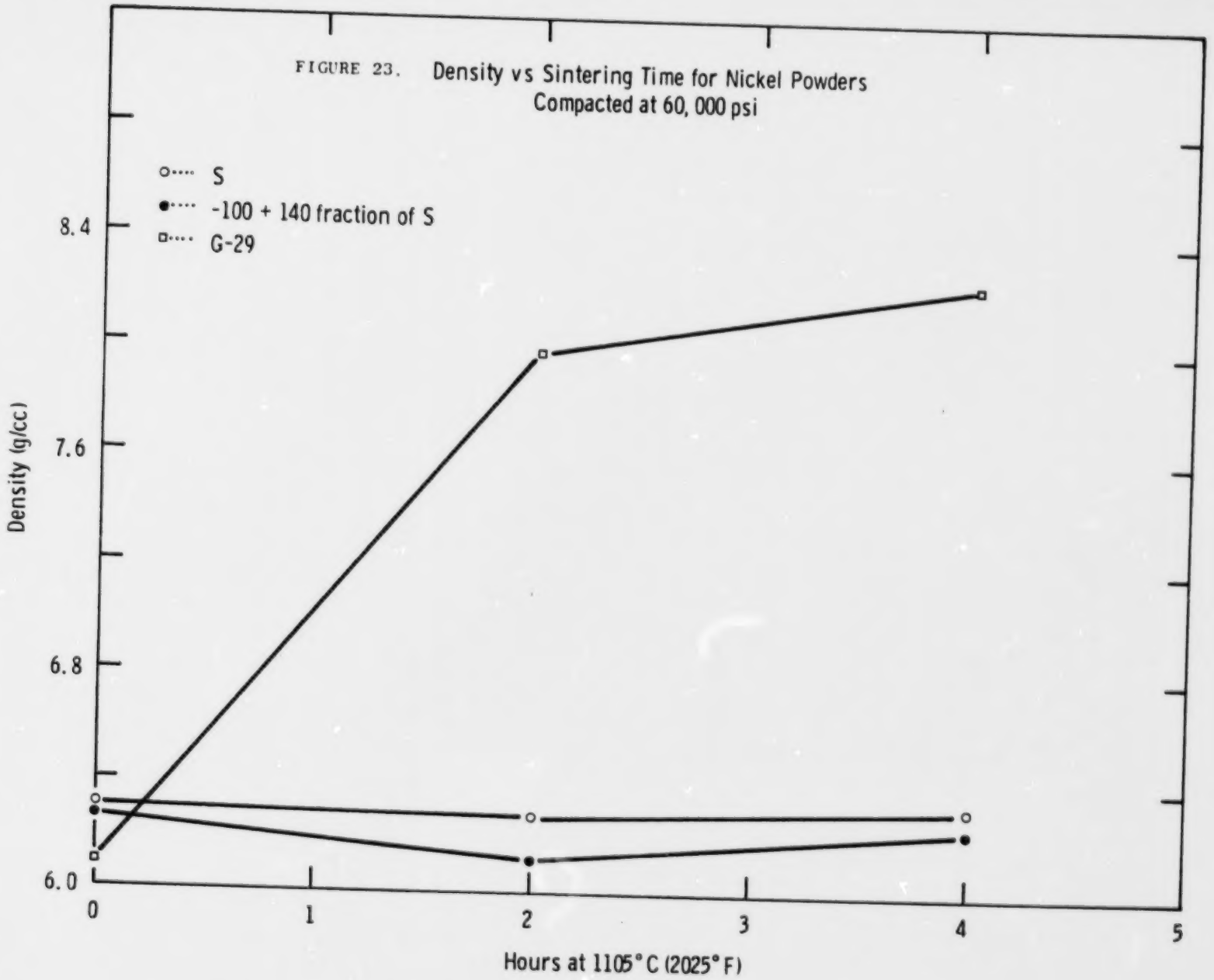

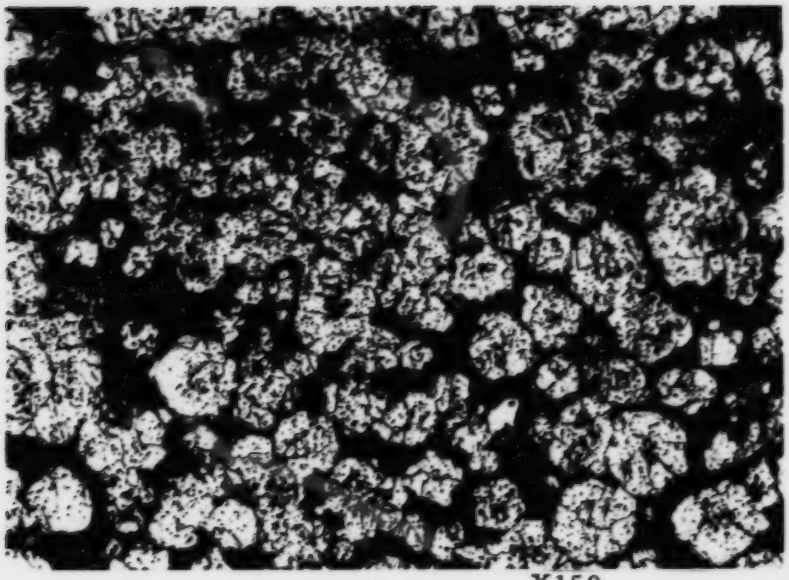

X150

(a)

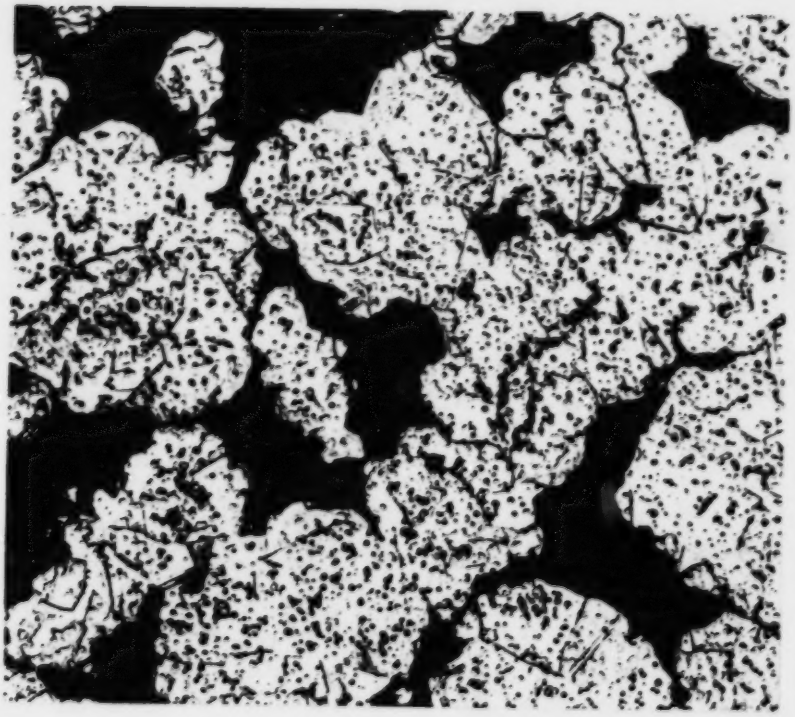

X400

(b)

Figure 24. Microstructure of S grade nickel powder. Compacted at 60,000 psi. Sintered at 1105°C (2025°F) for 2 hours. Etched.

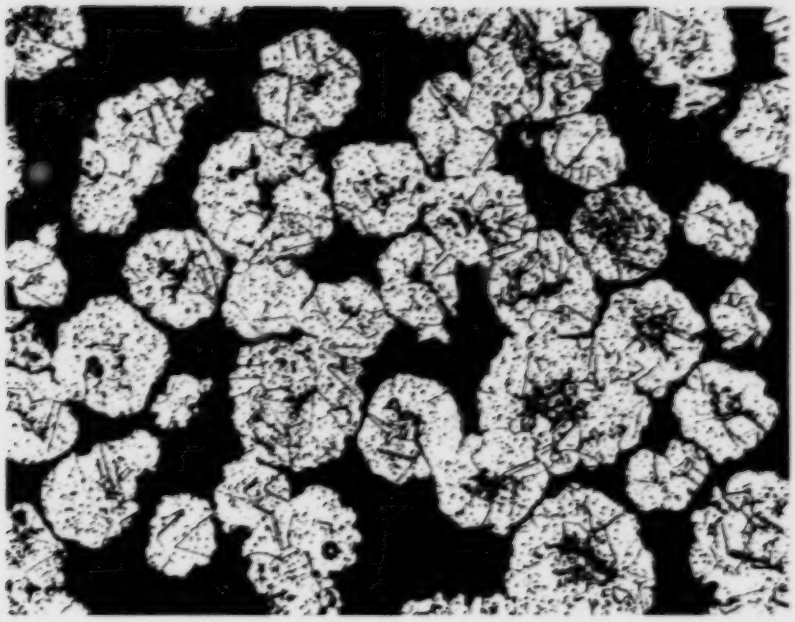

X150

(a)

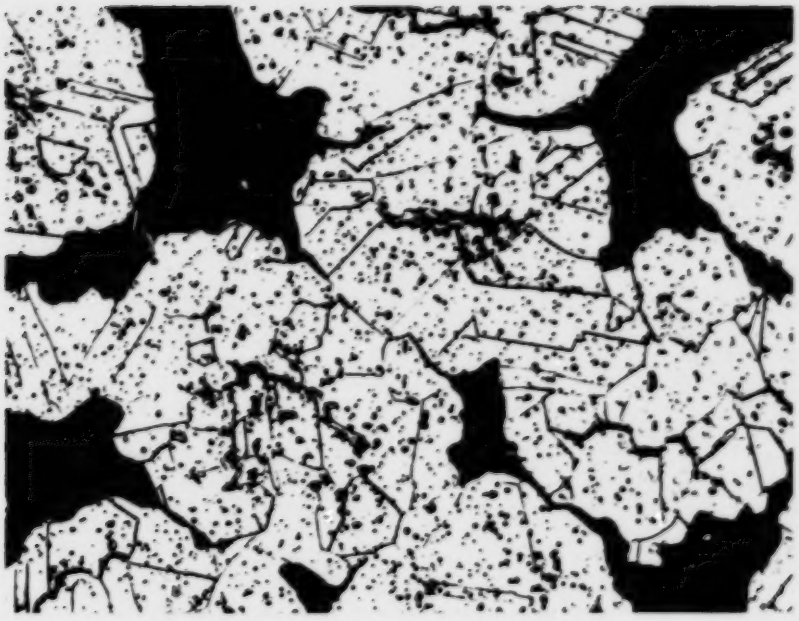

X400

(b)

Figure 25. Microstructure of -100 + 140 fraction of S grade nickel powder. Compacted at 60,000 psi. Sintered at 1105°C (2025°F) for 2 hours. Etched.

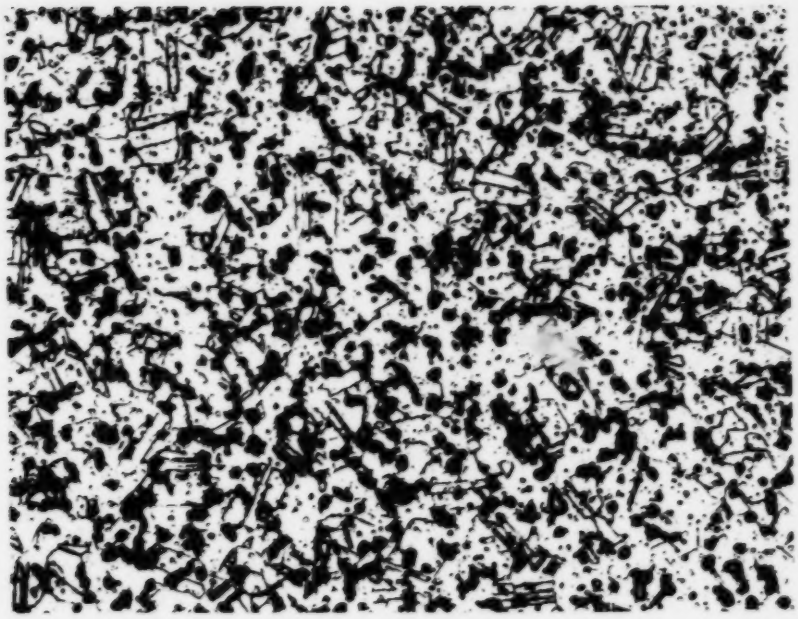

X400

(a) 2 hour sinter.

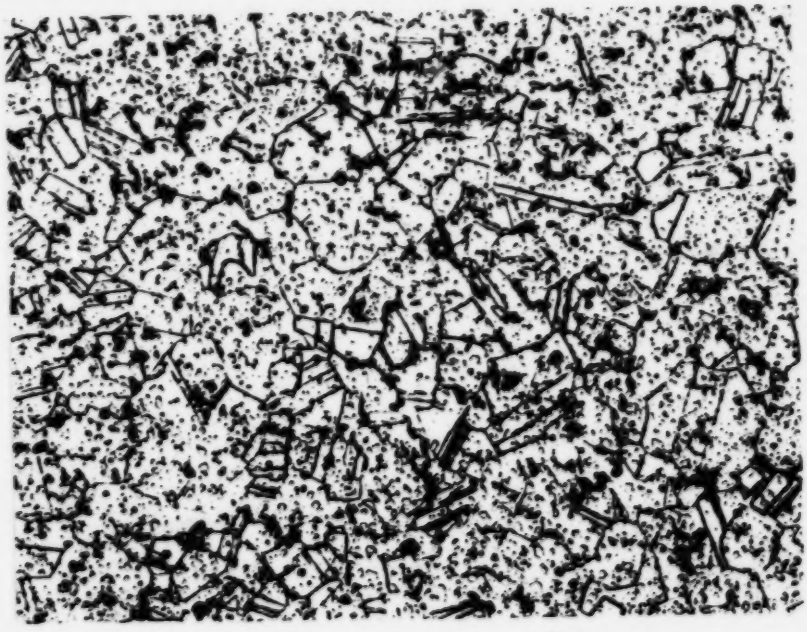

X400

(b) 4 hour sinter.

Figure 26. Microstructure of G-29 grade nickel powder. Compacted at 60,000 psi. Sintered at 1105°C (2025°F) for above times. Etched.